

Accepted Manuscript

Online assessment of TiC decomposition in laser cladding of metal matrix composite coating

Muvvala Gopinath, Debapriya Patra Karmakar, Ashish Kumar Nath



PII: S0264-1275(17)30195-8
DOI: doi: [10.1016/j.matdes.2017.02.061](https://doi.org/10.1016/j.matdes.2017.02.061)
Reference: JMADE 2801

To appear in: *Materials & Design*

Received date: 25 December 2016
Revised date: 11 February 2017
Accepted date: 18 February 2017

Please cite this article as: Muvvala Gopinath, Debapriya Patra Karmakar, Ashish Kumar Nath , Online assessment of TiC decomposition in laser cladding of metal matrix composite coating. The address for the corresponding author was captured as affiliation for all authors. Please check if appropriate. *Jmade*(2017), doi: [10.1016/j.matdes.2017.02.061](https://doi.org/10.1016/j.matdes.2017.02.061)

This is a PDF file of an unedited manuscript that has been accepted for publication. As a service to our customers we are providing this early version of the manuscript. The manuscript will undergo copyediting, typesetting, and review of the resulting proof before it is published in its final form. Please note that during the production process errors may be discovered which could affect the content, and all legal disclaimers that apply to the journal pertain.

Online assessment of TiC decomposition in laser cladding of metal matrix composite coating

Muvvala Gopinath, Debapriya Patra Karmakar, and Ashish Kumar Nath*

Department of Mechanical Engineering, Indian Institute of Technology, Kharagpur, India

Abstract

Decomposition of ceramic particles in metal matrix composite coatings developed by laser cladding process is one of the major problems that deteriorate the mechanical properties of coating. Further, a large number of process parameters involved in laser cladding makes the process optimization difficult. Therefore, a study was undertaken to assess the condition of TiC particles in the molten pool by monitoring the thermal history using an IR pyrometer. It was observed that with the increase of molten pool lifetime, a reaction layer is created between TiC particles and metal matrix which improves their bonding. However, with further increase in the molten pool lifetime TiC particles were found to decompose completely forming dendritic structure in the metal matrix through heterogeneous nucleation and subsequent crystallization during the solidification process. This results in a change of the solidification shelf slope which can be used as an effective signature to assess the TiC particle condition in molten pool online without performing any destructive test. The modified structure of metal matrix exhibited brittle nature which increased the wear rate due to fracture and spalling of coating during the wear test.

Keywords: *Laser cladding, IR pyrometer, online monitoring, molten pool thermal history, decomposition.*

*Corresponding Author: Tel: +91 - 3222 – 281784; fax: +91-3222-25530

E-mail address: aknath@mech.iitkgp.ernet.in

Postal address: Department of Mechanical Engineering, IIT Kharagpur, Kharagpur-721302, India

1. Introduction

Metal matrix composite (MMC) coatings have drawn much attention of industries to meet the increasing demand on component life. Ceramic-reinforcement in metal matrix improves the tribological properties, stiffness, specific strength, high temperature creep behaviour and hot corrosion resistance [1-4]. Metal matrix is selected on the basis of intended application and environment, wherein the improvement in wear resistance is realised by mixing various carbides in the metal matrix. MMC coating can be obtained by many processes, like gas tungsten arc cladding [5], plasma spraying [6], laser cladding [1], and high velocity oxygen fuel spraying (HVOF) [7], etc. With the advancement of high power lasers and emerging additive manufacturing technology, the laser cladding process is becoming more popular. Further, the process is more flexible with minimum dilution, distortion and heat affected zone compared to other processes. Also, this produces extremely refined microstructure through rapid solidification and cooling by self quenching mechanism.

In MMC coatings, while the ceramic particles support the externally applied load, the matrix binds the particles and transfers the external load to individual particles. Improper wetting between matrix and ceramic particles results in premature failure of the coating through particle pull out under rubbing action. Also, the interface between ceramic particle and metal matrix acts as crack initiation point under dynamic loading [8-11]. Therefore, a proper interface is required to transfer the load, which dictates the performance of a MMC coating. The wetting procedure is kinetic and depends on the temperature and hold time of ceramic particles in the molten matrix. In other words, wetting between ceramic particles and metal matrix depends on the thermal history of the molten pool. Allowing proper hold time and / or cooling rate initiates a reaction layer between solid particle surfaces and molten metal matrix enhancing the wettability [12]. Hong et al. [13] studied the influence of laser line energy (J/mm) on constitution phases, microstructure and wear performance of laser deposited TiC / Inconel 718 composite coating. It was reported that the reaction layer thickness between TiC particles and metal matrix increased with the increase of line energy. However, at relatively higher line energies which result in slower cooling rates, TiC particles are found to decompose. Further, slow cooling rates may also cause elemental segregation in Inconel 718 forming Laves phase [14] which deteriorates the mechanical properties. Thus, there exists an optimum window of process parameters in which a sound quality of coating with good wetting and without any decomposition can be obtained. However, as various process parameters like laser beam intensity profile, laser wavelength, cladding head / nozzle design, etc. are system dependent, the same optimized process parameters may not reproduce

the desired results elsewhere. Further, laser cladding process with blown powder method involves more than 19 process parameters [15] which make the parametric optimization more complex.

Most of the existing studies in the field of MMC coatings are based on post analysis i.e. after deposition samples are cross-sectioned, polished, etched and analysed for microstructural and phase changes with microscopes and XRD respectively, which is time consuming. The present study focuses on identifying the change in phase of ceramic particles in laser cladding process by monitoring the thermo-cycle that molten pool undergoes using an IR pyrometer, and correlating the changes in microstructure with the molten pool lifetime. By reproducing the same molten pool thermal history, the results could be replicated elsewhere, independent of laser processing system.

Molten pool in laser cladding process experiences rapid thermo-cycles i.e. fast heating and cooling, and this demands for a monitoring system with fast acquisition time, capable of detecting the temperature from a small processing zone. Several studies demonstrated the application of photodiodes, CCD cameras, acoustic sensors and pyrometers in laser material processing [16, 17]. Smurov and co-researchers [17-22] carried out extensive research on monitoring the laser cladding process using IR pyrometer. They developed a two wavelength pyrometer and studied the effect of various process parameters like laser power, scan speed, powder mass flow rate, laser pulse shape etc. on temperature signal during the laser cladding process. Bi et al. [24-26] developed a novel laser cladding head integrated with different sensors like photodiode, CCD camera and IR pyrometer for monitoring and controlling the process. They also reported the dependency of measured temperature signal on process parameters. In multilayer thin wall deposition, the heat conduction mechanism transforms from 3 dimensions to 2 dimensions as the number of layers increases, which results in heat accumulation and non-uniform wall thickness. Moreover, absence of material at the edges to conduct the heat results in edge build up as well as shrinkage of the wall. The authors further extended their work in which laser beam power was varied during the process with the change in IR-temperature signal from a pre-set value using a PID controller based closed loop control system to get uniform multilayer deposition [26]. Most of the existing studies are based on monitoring the average peak temperature of molten pool and its variation with process parameters. However, the microstructure depends on the whole thermo-cycle of the molten pool. Therefore, in the current study molten pool thermo-cycle has been monitored using an IR pyrometer in preplaced powder laser cladding. This method could be adapted in blown powder method also.

The nickel and titanium based super alloys have gained immense popularity as engineering materials in recent times because of their outstanding properties which include retention of strength and chemical stability at high operating temperatures [13, 27-31]. Some of their properties are further strengthened by mixing ceramic particles forming metal matrix composites. In the present study Inconel 718, a nickel based super alloy has been selected as the metal matrix. Its hot corrosion, oxidation and wear resistance and fatigue properties make it an attractive candidate for many applications such as gas turbines, high speed air frame parts, rocket motors, nuclear reactors, components which operate at high temperatures (~700 °C) [32-34]. Different types of ceramic particles, e.g. WC, TiC, VC, Al₂O₃, SiC, TiN, Cr₂O₃, and CrC etc. are commonly used in metal matrix composite coatings [1, 5, 12, 13, 35, 36]. Among these, TiC has sparked considerable interest because of its relatively low density, good wettability, chemical compatibility, high modulus and rather high flexural strength along with high hardness and wear resistant properties [35, 36]. Therefore, in the current study TiC is selected for hard phase reinforcement in Inconel 718 matrix. AISI 304 austenitic steel has been used as a substrate material in this study which is widely used in oil, nuclear, chemical and other industries due to its excellent corrosion resistance, good mechanical properties and acceptable machinability. However, they usually exhibit poor sliding wear resistance and hardness which may result in material transfer, mechanical mixing and oxidation between double sliding bodies [37-39] which needs to be improved. Therefore, in the current study it has been selected as substrate material to improve wear resistance by depositing the MMC coating

2. Experimental setup

AISI 304 austenitic steel specimens of 50 mm × 50 mm × 6 mm dimensions with their top surface abraded with 200 mesh size SiC grit paper, followed by ultrasonic cleaning were laser cladded with 70:30 wt% powder mixture of Inconel 718 and TiC. The particle size of Inconel 718 and TiC powder was in the range of 43-100 μm and 5-20 μm respectively having morphology as shown in Fig. 1(a) and (b). Chemical compositions of substrate and clad materials are presented in Table 1. Inconel 718 and TiC were mixed mechanically by alternate cycles of mechanical stirring (Spinot Model MC-02, Tarsons) in aqueous solution of 2% polyvinyl alcohol (Alfa Aesar, 87–89% hydrolysed), making it into a thick slurry. The slurry was coated on to the substrate using a coating machine (Model no: K101 control coater, RK Print Coat Instruments Ltd., UK,) to form a uniform layer of 1mm thickness. The

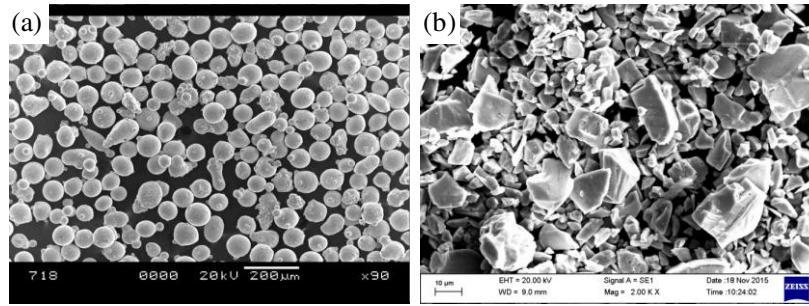


Fig. 1. Morphology of (a) Inconel 718 and (b) TiC powder

Table 1

Chemical composition (Wt%) of cladding and substrate materials

Element (Wt%)	Cr	Fe	Nb	Mo	Al	Ti	Mn	Si	B	Ni	C	P	S
IN 718	19.02	18.1	4.92	3.19	0.54	0.97	0.04	0.20	0.004	Bal.	-	-	
AISI 304	18.97	Bal.	-	0.224	-	-	1.731	0.753	-	8.554	0.067	0.045	0.031

Table 2

Laser cladding process parameters

CW mode			
Laser beam power (W)	Scan speed (mm/min)	Thickness of preplaced powder coating (mm)	Beam spot diameter (mm)
1200	200 - 1200	1	3

coated substrate was baked in a furnace at 150 °C in argon environment for 15 min to remove moisture from the coating and for proper bonding, and then cooled to room temperature in the furnace.

Laser cladding was carried out using a 2 kW Yb-Fibre laser (IPG photonics, Model no. YLR 2000), operating at 1.07 μm wavelength. The laser has multimode beam intensity profile with high intensity at the centre and two annular rings of relatively low intensities [40]. It can be operated in both CW as well as modulated mode at 50-1000 Hz frequency and 5-100% duty cycle. In modulated mode the experimentally measured rise and fall times (10% to 90%) during pulse ‘ON’ and ‘OFF’ are about 25 μs and 600 μs respectively. The beam delivery system is mounted on a 5-axis CNC machine which can move at speeds up to 20 m/min. Argon gas was used for both shielding and shrouding to protect the optical components of beam delivery system from fumes and to shield the molten pool from oxidation respectively. Shrouding gas was provided laterally at 5 l/min flow rate through a 6

mm diameter copper tube. Table 2 shows the process parameters for the laser cladding experiment.

The laser clad tracks were cross-sectioned using a wire-cut EDM, mirror polished and analysed under SEM to study the condition of TiC particles in the metal matrix. Fracture test was carried out to study the effect of decomposition of TiC on mechanical properties (ductility) of the metal matrix. For carrying out the fracture test, single tracks were dissected along the length from three sides using wire-EDM to expose the clad track alone in the tensile test. Wear test was also carried out on the clad surface developed with 30% overlapped tracks, using a ball on disk setup (Make: DUCOM, TR-201-M3). WC ball was used as a counter body and wear test was carried at 300 RPM over a 5 mm diameter circular track with 19.62 N load for 15 min.

2.1 Calibration of IR pyrometer

The thermo-cycle of the molten pool was monitored using a single spot monochromatic pyrometer (Micro Epsilon, model: CTLM-2HCF3-C3H) operating at 1.6 μm wavelength, having acquisition time, vision zone and accuracy of 1 ms, 0.7 mm diameter and $\pm (0.3\% \text{ of reading} + 2^\circ\text{C})$ respectively, and temperature measurement range of 385-1600 $^\circ\text{C}$. The pyrometer is focused on the substrate by placing it at a distance of 200 mm from the substrate and an angle of 20° with respect to the incident laser beam to monitor temperature of a small zone on the laser cladding track. This was kept stationary during the experiment, while the laser beam was scanned over the substrate passing through the temperature monitoring zone. Though the pyrometer is specified to measure 1.6 μm wavelength radiation it was experimentally observed that it also detects the 1.07 μm wavelength laser radiation scattered / reflected from the substrate, thus giving an erroneous temperature signal. Fig. 2 shows a typical thermo-cycle that was recorded with the pyrometer while the laser beam was scanned over a bare AISI 304 substrate at 700 W laser power and 9000 mm/min scan speed. The dwelling time of 3 mm diameter laser beam over 0.7 mm diameter vision zone of the pyrometer under this scanning condition is ~ 25 ms, according to eq. 1. The rise time of the pyrometer temperature signal is expected to be nearly the same. However, it is observed from Fig. 2 that the rise time, which is the duration between the point θ and C is much longer, about 132 ms. This temperature signal is recorded at a middle zone of 50 mm wide substrate while laser beam was scanned across it. Further, with no sign of surface melting, the recorded temperature is above the melting point of AISI 304 austenitic steel ($\sim 1400^\circ\text{C}$). From these

observations, it was concluded that the IR pyrometer detects the 1.07 μm wavelength laser radiation reflected from the substrate along with the 1.6 μm meant for monitoring the temperature.

$$\text{Dwelling time } t = \frac{(\text{Laser beam spot diameter} + \text{pyrometer vision zone})}{\text{Scan speed}} \quad (1)$$

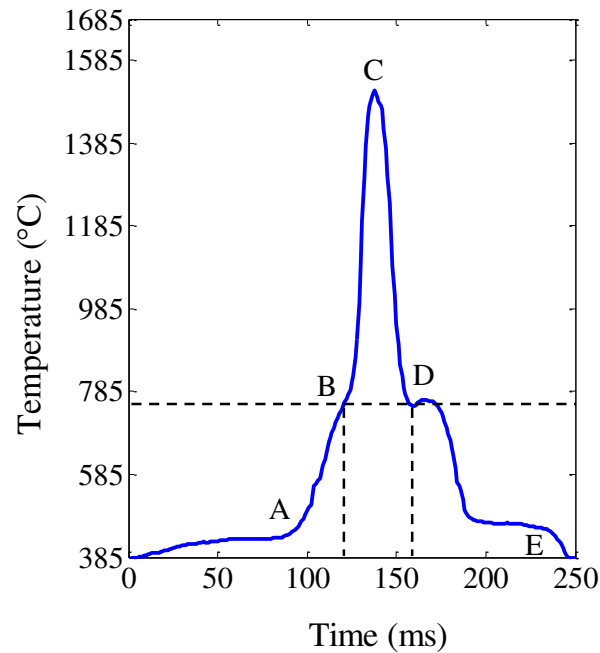


Fig. 2. Thermo-cycle recorded using IR pyrometer (700 W laser power, 9000 mm/min, 3 mm spot diameter)

The detected signal shown in Fig. 2 can be divided into different sections i.e. OA , AB , BC , CD and DE based on the slope of temperature profile. It is observed that the duration of BC is close to the expected interaction time, which indicates that BC is the signal from the zone of interest. It is also observed that the duration of OB and DE is equal, from which it can be concluded that OB and DE are the signals caused by the laser radiation reflected from an equal extent of the trailing and leading end of the zone of interest respectively. The same conclusion could be drawn from the trend observed in the thermo-cycles for different scan speeds as shown in Fig. 3.

In order to block the reflected laser radiation from entering into the pyrometer, a narrow band notch filter of 1064 ± 25 nm spectral range with optical density of 3 was mounted in front of the pyrometer. Fig. 4 shows the temperature signal obtained with the notch filter at 700 W laser power and 2000 mm/min scan speed. With this scan speed the calculated dwell time of the laser beam over the vision zone is ~ 110 ms. However, the temperature signal reaches to peak in ~ 70 ms. It is also observed that the measured peak

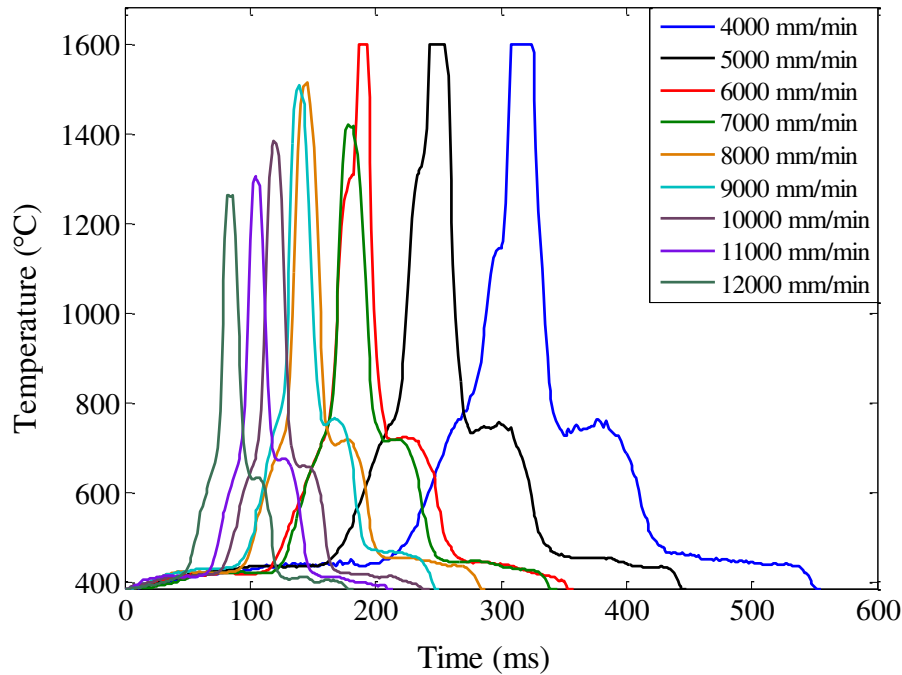


Fig. 3. Typical profile of thermo-cycles (Without notch filter, 700 W, 3 mm spot diameter)

surface temperature has reduced drastically with no sign of laser radiation effect on the temperature signal profile. In spite of surface remelting observed in this case, the temperature monitored was much below the melting point. This could be due to the blocking of some part of 1.6 μm radiation signal along with the 1.07 μm wavelength laser radiation by the notch filter. This would not allow the pyrometer to detect temperatures in the lower range which is also apparent from the relatively shorter temperature rise time compared to the estimated value. Therefore, the IR pyrometer was suitably calibrated to obtain the actual temperature. In order to calibrate the pyrometer, molten pool was created on the surface of three different materials i.e. Al, Cu and SS 304 having melting point at ~ 660 $^{\circ}\text{C}$, ~ 1080 $^{\circ}\text{C}$ and ~ 1400 $^{\circ}\text{C}$ using a stationary laser beam and the thermo-cycles were recorded, which are shown in Fig. 5. In each of these cases, solidification shelf location was identified as shown in Fig. 5 from which the recorded melting point was obtained and the actual melting point was divided to calculate the calibration factor 'a'. From the solidification shelf of SS 304 and Cu, the value of 'a' is obtained as 2.04 and 2.02 respectively. This small difference could be due to the slight variation in actual melting point from the assumed melting point because of the presence of impurities. With this calibration factor, the temperature monitoring range of the IR pyrometer with the notch filter changes from 385-1600 $^{\circ}\text{C}$ to ~ 785 -3260 $^{\circ}\text{C}$. Since the melting point of Al is below this range, no solidification shelf could be observed in this case. Similar to the above procedure, the pyrometer was calibrated for the melting point of Inconel

718 and monitored temperature signals during laser cladding were readjusted to obtain their actual magnitudes.

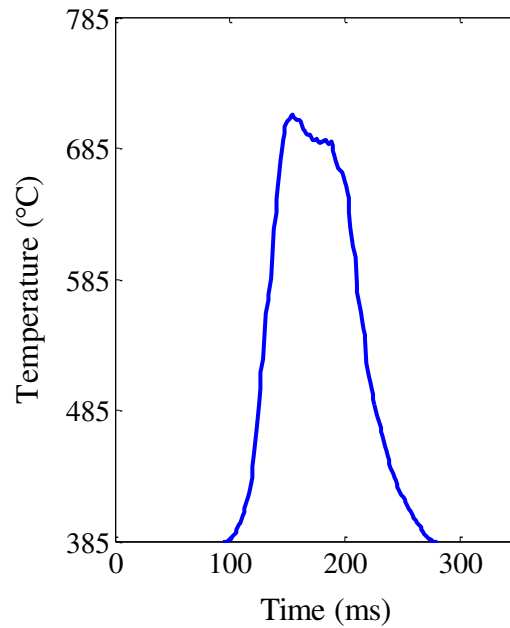


Fig. 4. Temperature signal recorded with notch filter (700 W, 2000 mm/min and 3 mm beam spot diameter)

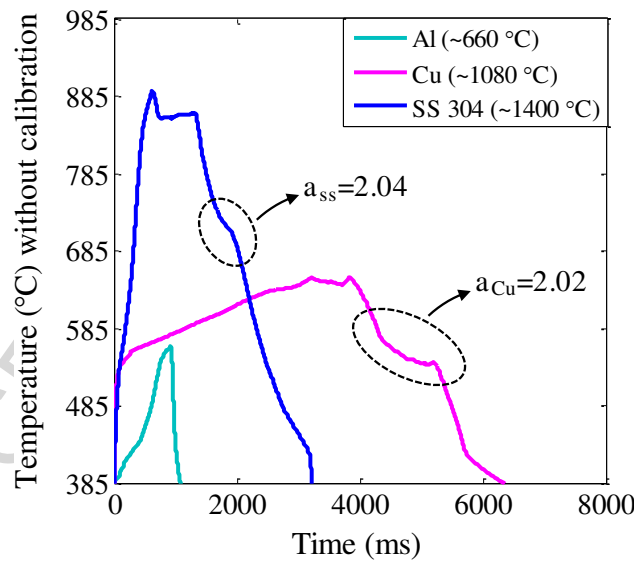


Fig. 5. Thermo-cycle of molten pool in case of Al, Cu and SS 304

2. Results and Discussion

In the present laser cladding process, a high power focused laser beam scans over the preplaced powder melting the powder layer along with a thin top surface layer of the substrate, which after the passage of laser beam solidifies and bonds to substrate. Thus, the preplaced powder layer undergoes a heating cycle (*OB*) and a cooling cycle (*BF*) as shown in

Fig. 6, during which melting and solidification takes place respectively. This thermo-cycle is going to dictate the formation of different phases and mechanical properties of the coating/component. Heating cycle can be further divided into two zones OA and AB . OA is the period during which heating and melting takes place, and the molten pool temperature keeps on rising as the laser beam dwells over the vision zone of the pyrometer. Beyond a certain temperature molten metal starts vaporising as well heat loss due to conduction, convection and radiation becomes significant restricting further rise in temperature [41]. During this period of laser dwelling the molten pool temperature remains nearly constant in a quasi-steady state (AB). As the laser beam proceeds, the molten pool behind it starts cooling; initially a steep drop in temperature (BC) takes place while the pool remains in liquid state. Points 'C' and 'E' represent the liquidus and solidus temperature of the material between which nucleation starts, initiating solidification and ends as the solidus temperature is reached. The zone between CE is generally termed as solidification shelf or freezing zone. It may be noticed that the zone CE is having two distinct zones CD , where the slope of the solidification shelf is reduced to almost zero and DE whose slope is less steep compared to BC . This could be due to the mixing of two materials which are having different melting points resulting in solidification of one having higher melting point initially, TiC in the current study, followed by the other (Inconel 718) having lower melting point. The change in the slope of cooling curve is due to the release of latent heat of fusion. The duration between BE represents the molten pool lifetime. This is followed by solid phase cooling EF which

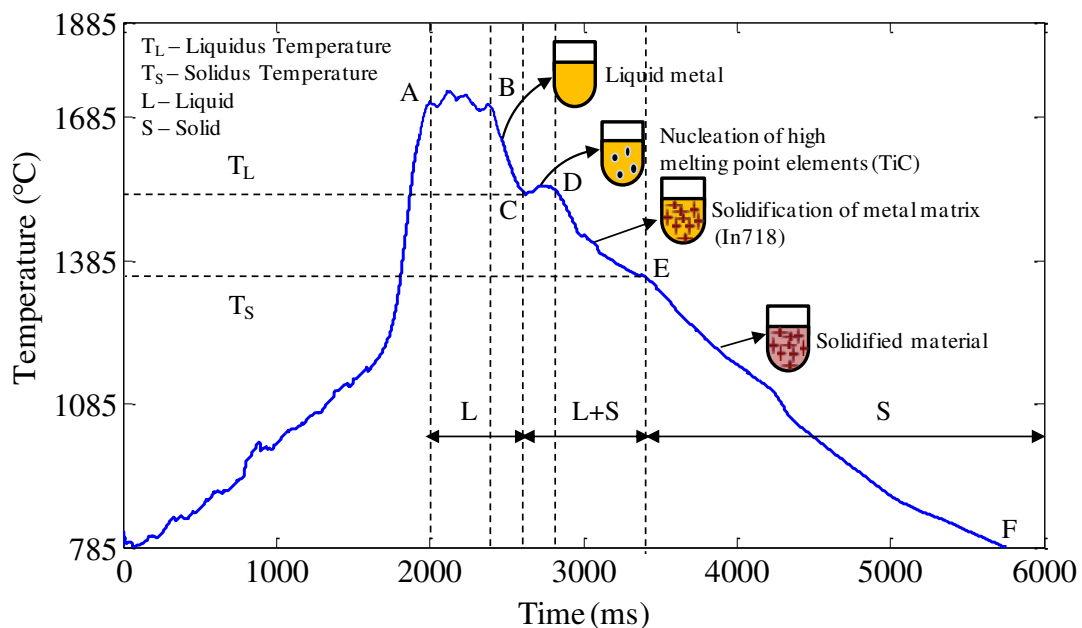


Fig. 6. Typical thermo-cycle recorded during laser cladding of Inconel 718 + TiC at 1200 W laser power and 200 mm/min scan speed

dictates the formation of precipitates, grains size and different phases like in case of laser transformation hardening.

3.1 Identification of change in phase

In order to identify the effect of TiC particles inclusion in Inconel 718 on temperature signal, laser cladding was carried out with and without TiC particles. Fig. 7 shows the thermo-cycles recorded in both the cases at 1200 mm/min (Fig. 7a) and 400 mm/min (Fig. 7b) scan speeds. Laser power and beam spot diameter were kept constant at 1200 W and 3 mm respectively. In case of 1200 mm/min, it can be seen that the presence of TiC in metal matrix of Inconel 718 resulted in an increase of molten pool temperature as shown in Fig. 7a, which is attributed to the exothermic reactions that occur in the molten pool. Further, the steepness of cooling curve of the molten pool is more in case of Inconel 718/TiC compared to that in Inconel 718 alone. However, in both the cases solidification shelf was located at the same temperature as highlighted in Fig. 7a. Fig. 7b shows the thermo-cycle during laser cladding at 400 mm/min where one can identify the difference in both the cases. Liquidus temperature of the material was found to shift from 1400 °C in Inconel 718 to 1550 °C in Inconel 718/TiC. Further, the slope of solidification shelf was found to be changing almost from near 0° in case of Inconel 718 to ~70° with the addition of TiC. In general, pure metals exhibit a zero slope solidification shelf. In case of a binary system same will exist at the extreme ends of the phase diagram i.e. at 100% of element A or B and also at a particular composition yielding a eutectic point where solidification takes place at a single temperature. Inconel 718, though a

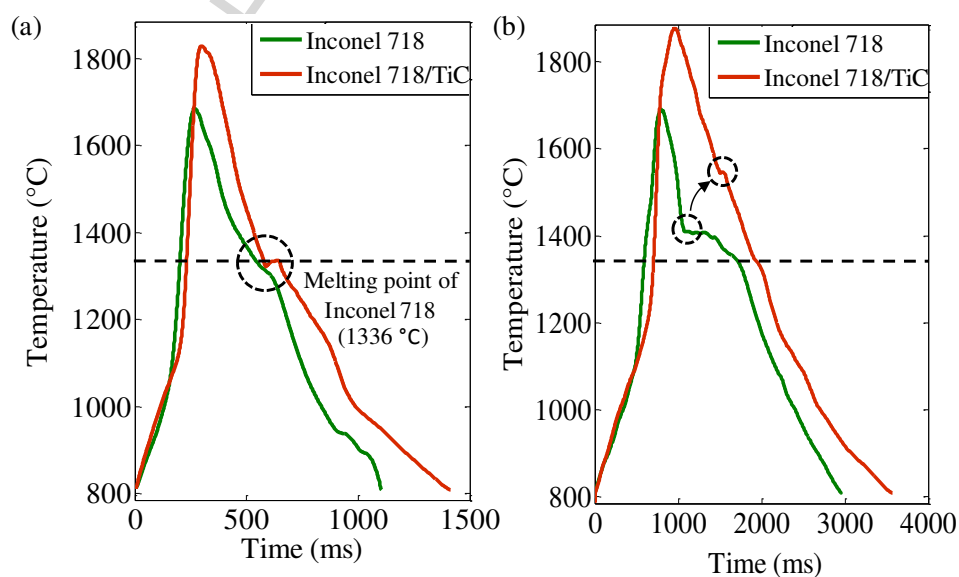


Fig. 7. Thermo-cycles during laser cladding of Inconel 718 and Inconel 718 + TiC at 1200 W laser power, (a) 1200 mm/min and (b) 400 mm/min

super alloy consisting of nearly 10 alloying elements (Table 2) was found to exhibit solidification shelf having near zero slope. The same was maintained even with addition of TiC particles at relatively higher scan speed i.e. at 1200 mm/min, 1000 mm/min and 800 mm/min. However, at slower scan speeds solidification shelf exhibited a slope indicating the solidification process taking place over a range of temperature which could be due to the change in physical composition of Inconel 718 with addition of TiC. In order to confirm the postulates, the clad tracks were cross-sectioned and microstructures were analysed under scanning electron microscope. Fig. 8 shows the microstructure and corresponding thermo-cycles of samples clad at 1200 W laser power and two different scan speeds of 1200 mm/min and 400 mm/min. A clear change in microstructure is evident from Fig. 8. For slower cooling at the lower scan speed, TiC particles are found to decompose exhibiting a dendritic structure in the matrix causing compositional changes which in turn causes a change in the solidification shelf slope and its location. However, in case of 1200 mm/min, it can be observed that TiC particles were intact with no sign of decomposition and solidification shelf remained same as that of Inconel 718, Fig.7a. Thus, the thermo-cycle of molten pool could be utilized for non-destructive analysis of compositional changes as well as decomposition of ceramic particles in MMC coatings.

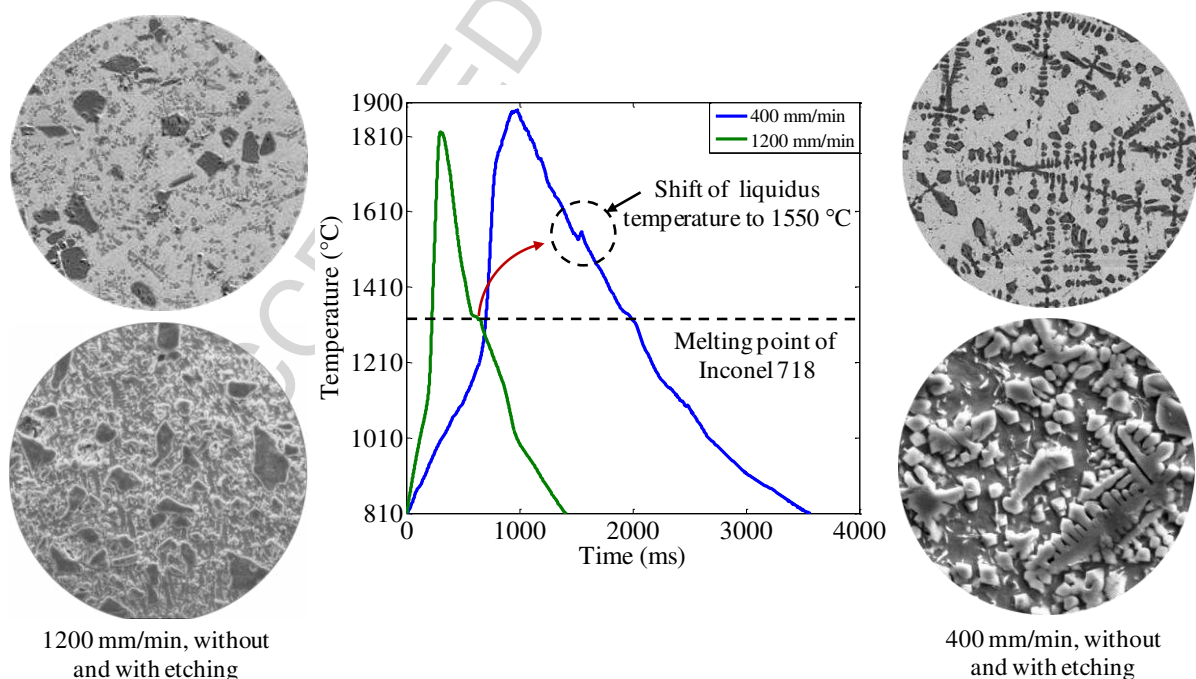


Fig. 8. Relation between slope of solidification shelf and microstructure

3.2 Molten pool thermal history and its affect on microstructure

Fig. 9 shows the influence of scan speed on different aspects of molten pool thermal history, which are associated with cooling cycle and dictate the resulting microstructure and mechanical properties of the formed clad layer. The lifetime of molten pool and solidification shelf, both decrease with the increase of scan speed (Fig. 9a), while the cooling rate increases (Fig. 9b). Similar trend was reported by the simulation results of Zhang et al. [42]. In the current study, with the decrease of scan speed, line energy increases from 60 J/mm to 360 J/mm, increasing the amount of energy coupling to the clad layer. Further, the slow scan speed causes substrate temperature to rise due to conduction of heat from the clad layer.

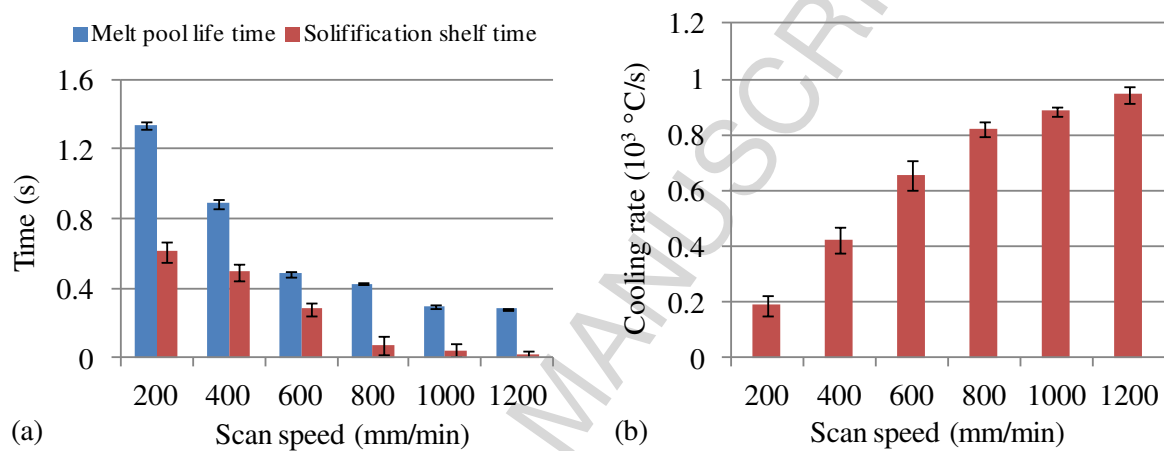


Fig. 9. Effect of scan speed on (a) Molten pool lifetime and solidification shelf lifetime and (b) cooling rate

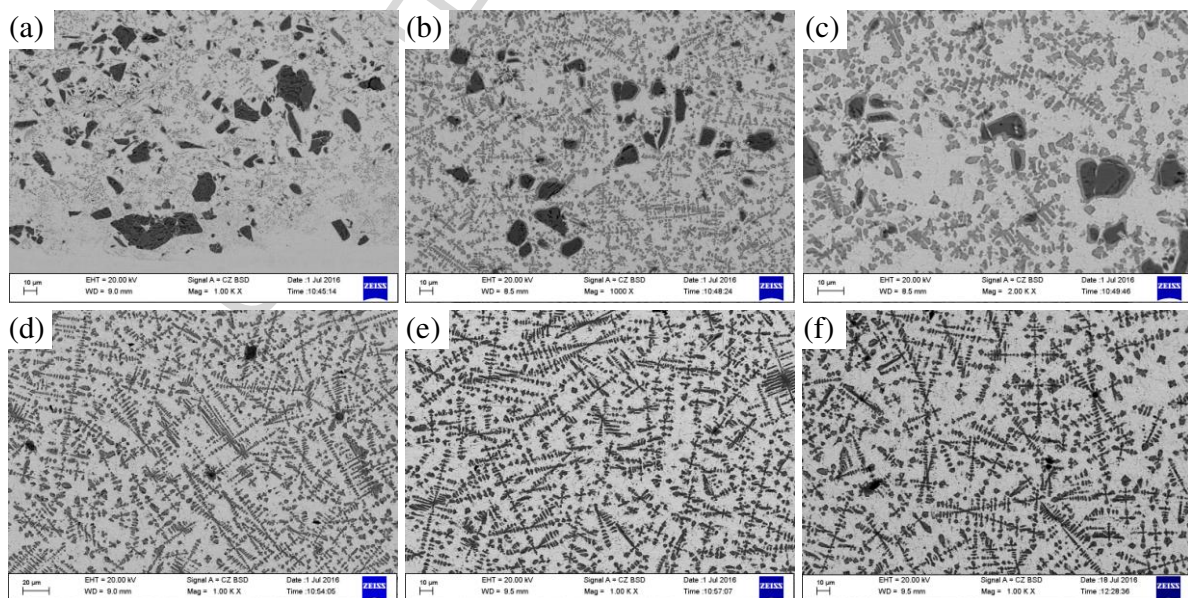


Fig. 10. Variation in microstructure with molten pool life time (a) 0.281 s, (b) 0.3 s, (c) 0.429 s, (d) 0.487 s, (e) 0.899 s and (f) 1.336 s

These two effects result in a decrease of temperature gradient between the substrate and the molten pool decreasing the cooling rate and increasing the molten pool lifetime as well as solidification shelf time. Exposing the ceramic particles to high temperatures for longer periods resulted in their decomposition as well as reaction with the metal matrix. Fig. 10 shows the variation in microstructure of clad layer with molten pool lifetime. The change in scan speed from 1200 mm/min to 200 mm/min resulted in increase of molten pool lifetime from ~0.281 s to ~1.336 s. It can be observed that at a higher scan speed where the molten pool lifetime is relatively short and rapid solidification takes place, ceramic particles are found to be intact (Fig. 10a) without undergoing any decomposition. With decreasing scan speed, as the molten pool lifetime increases from 0.281 s to 0.429 s, it is observed that the dendritic growth in metal matrix increasingly dominate with reduction in number of TiC particles due to their decomposition. In case of molten pool lifetime greater than 0.487 s (Fig. 10(d), (e) and (f)) TiC particles get completely decomposed. Further, the lengths of the dendritic core as well as secondary arms are found to increase with slower cooling.

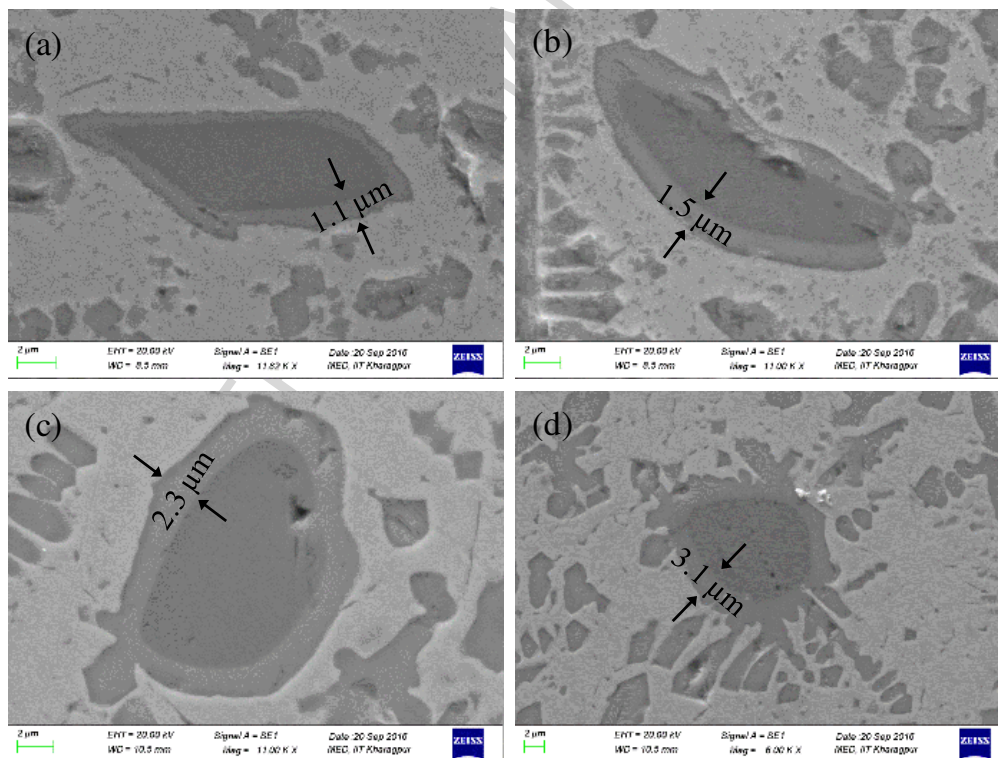


Fig. 11. Variation in reaction layer thickness with molten pool life time (a) 0.429 s, (b) 0.487 s, (c) 0.899 s and (d) 1.336 s

Fig. 11(a) - (d) shows the TiC particles in the metal matrix clad at 1200 W laser power and different scan speeds, 1200 mm/min, 1000 mm/min, 800 mm/min and 600 mm/min respectively. The molten pool lifetime corresponding to these speeds has been

presented in Fig. 9(a). It can be observed that a reaction layer between TiC and metal matrix is established in all these cases, which is desired for good wettability. Further, with the increase of molten pool lifetime, the reaction layer thickness gets increased as shown in Fig. 12; and at 600 mm/min the formation of dendritic growth and decomposition of TiC particle can be seen, Fig. 11d. The reaction layer is found to be rich in Nb and Mo which is evident from the EDS results presented in Fig. 13. As they have good affinity towards carbon they form secondary carbides. The thermodynamic equations (2) to (5) provide the information about possible reactions [43]. They show that the Gibbs free energy of Nb_2C is more negative than that of TiC supporting the segregation of Nb around the TiC particle. However, in case of fully grown dendrites as shown in Fig. 10(c), (d) and (e), the dendritic cores as well as the secondary arms were found rich in Ti and Nb as shown in Fig. 14. This indicates complete decomposition of TiC particle and formation of new secondary carbides of Nb and Ti via a dissolution/precipitation mechanism by means of the heterogeneous nucleation of TiC nuclei and subsequent crystal growth during the solidification process.

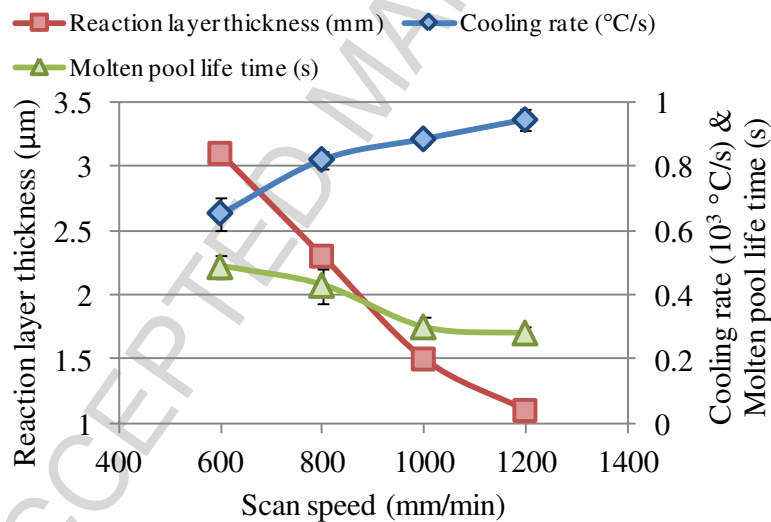


Fig. 12. Effect of scan speed on molten pool life time, cooling rate and reaction layer thickness

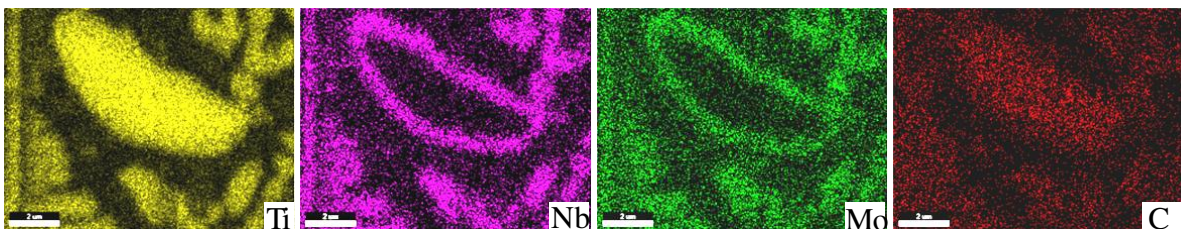


Fig. 13. Elemental mapping of TiC particle (1200 W, 1000 mm/min)

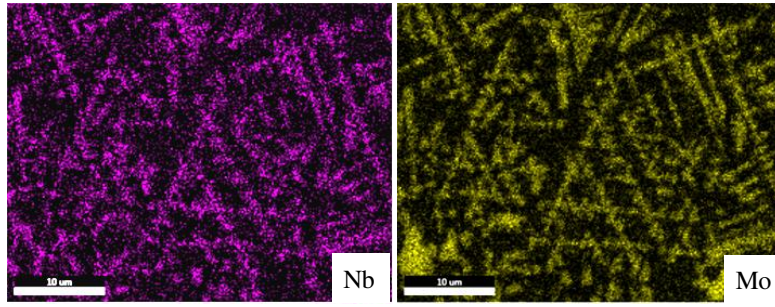


Fig. 14. Elemental mapping of Nb and Ti in fully grown dendritic structure (1200 W, 400 mm/min)

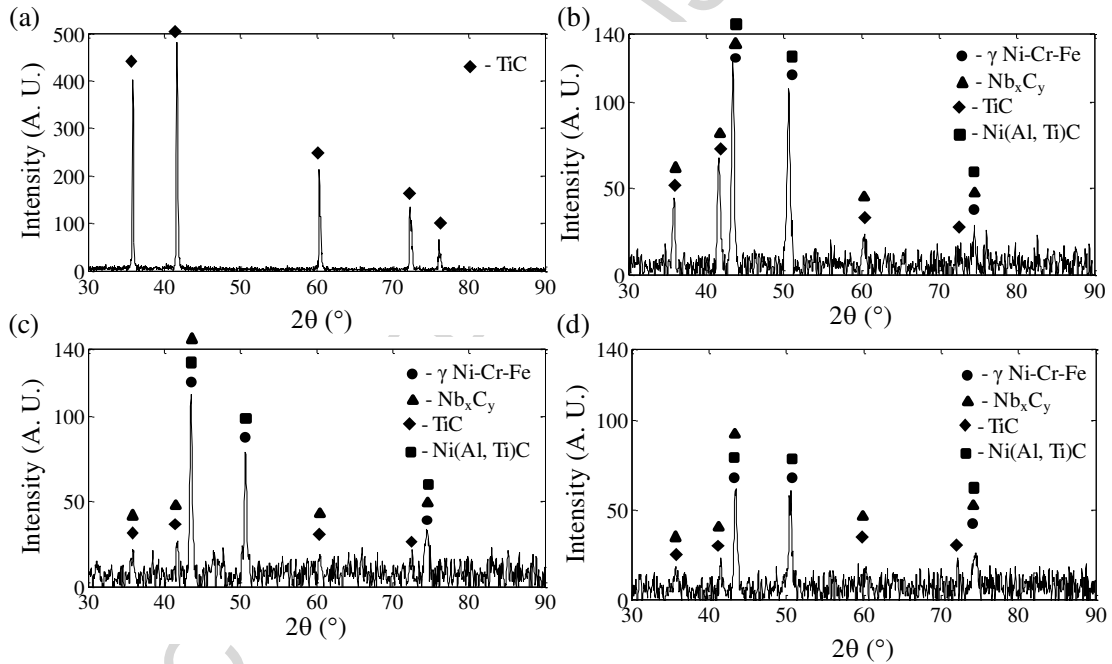
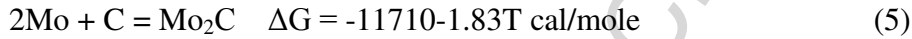
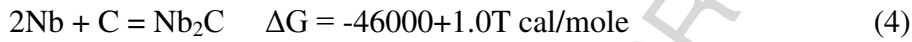
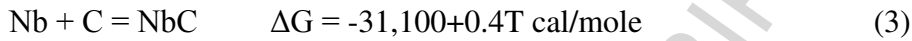
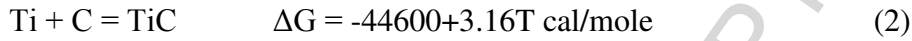


Fig. 15. XRD peaks of (a) TiC particles and clad tracks deposited at (a) 1200 mm/min, (b) 800 mm/min and (c) 400 mm/min

Different phases in the clad layer were identified using X-ray diffractometer with Cu $K\alpha$ radiation at 40 kV and 40 mA in continuous scan mode. A quick scan at $1.4^\circ/\text{min}$ was performed over a wide range of 30° – 90° . Fig. 15(a) - (d) shows the XRD peaks of TiC in samples clad at 1200 mm/min, 800 mm/min and 400 mm/min respectively. It can be seen that in case of 1200 mm/min scan speed XRD peaks of both Inconel 718 and TiC were strong; for instance one can consider TiC peaks at 35.902° and 41.707° and γ matrix peaks of Inconel 718 at 43.583° 2θ angle as shown in Fig. 15b. As the scan speed is reduced to 800

mm/min and 400 mm/min these peaks diminished indicating the decomposition of TiC forming secondary carbides, Fig. 15(c) and (d).

3.3 Mechanical properties of the coating

The effect of TiC decomposition on the mechanical properties of clad layer was analysed using fracture and wear tests. Fig. 16(a) and (b) shows the fractured surface of samples clad at 1200 W laser power and scan speeds of 1200 mm/min and 400 mm/min. In case of 1200 mm/min scan speed at which TiC particles were intact in Inconel 718 metal matrix, the clad layer exhibited ductile fracture. However, in case of 400 mm/min scan speed at which TiC particles were completely decomposed forming fully grown dendrites, the clad layer exhibited brittle fracture as shown in Fig. 16(b). The dissolution of TiC forming secondary carbides which are brittle in nature caused loss of ductility of Inconel 718 resulting in brittle fracture [44]. Fig. 17 depicts the effect of scan speed on the wear rate of clad surface developed with 30% overlapped clad tracks. The molten pool lifetime is also plotted in

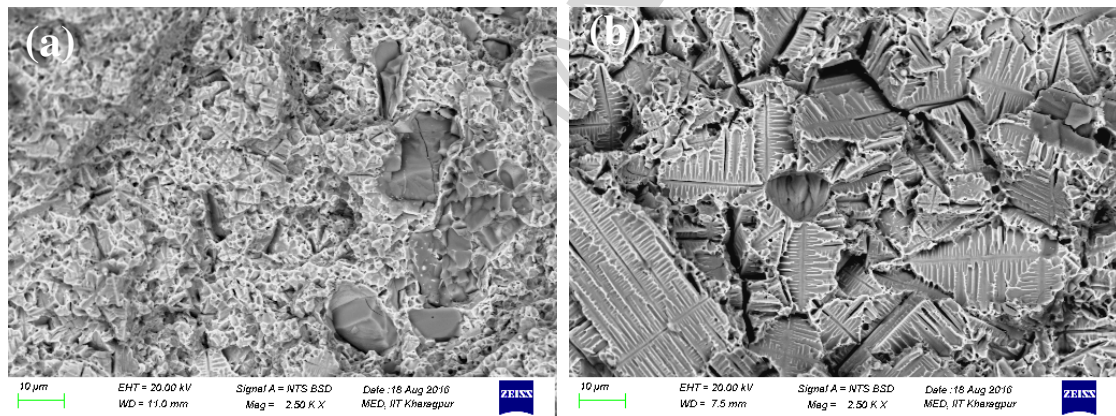


Fig. 16. Fracture surface of samples clad at 1200 W laser power and (a) 1200 mm/min and (b) 400 mm/min scan speed

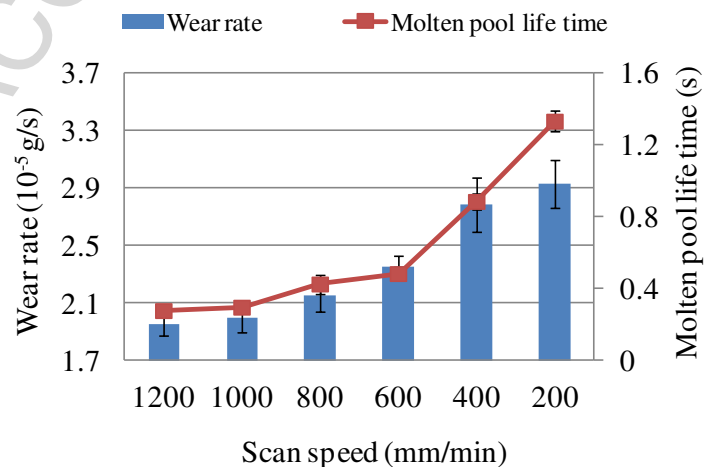


Fig. 17. Variation of wear rate with scan speed and molten pool lifetime

Fig.17. Both molten pool lifetime and wear rate increased with the reduction of scan speed. Thus, the clad surface which had longer molten pool lifetime exhibits relatively poor wear characteristics. Fig. 18 shows the wear surface and the debris morphology of samples clad at a laser power of 1200 W and scan speed of 1200 mm/min and 400 mm/min. It can be seen in Fig 18(c) and (d), in case of 400 mm/min scan speed the wear track exhibits significant fracturing and spalling of the surface resulting in increased wear rate; while in case of 1200 mm/min there is no sign of fracture or spalling, Fig 18 (a) and (b). This could be because of the brittle nature of coating resulting from the decomposition of TiC particles at the lower

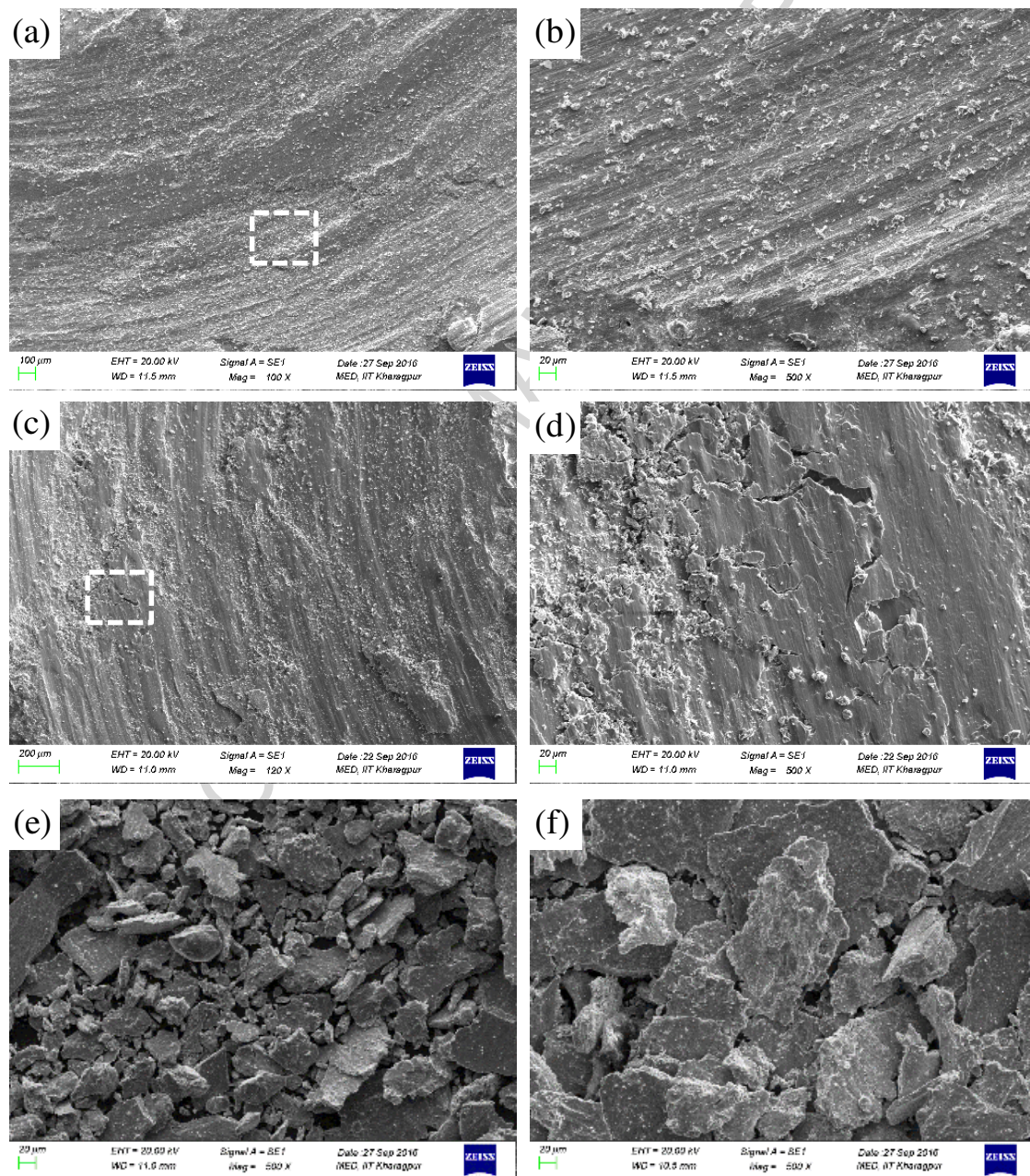


Fig. 18. SEM images showing typical wear surface morphology of samples clad at 1200 W laser power and (a), (b) 1200 mm/min and (c), (d) 400 mm/min scan speed and (e), (f) corresponding debris

scan speed leading to the modification of metal matrix. Further, it can be observed from the debris morphology presented in Fig. 18(e) and (f) for the two scan speeds that in case of 400 mm/min fracturing and spalling resulted in debris of larger size.

The current study demonstrated that the microstructure and phases, and the mechanical properties of the clad layer have good correlation with the melt pool lifetime and solidification shelf time that are reflected in the thermo-cycle of the clad layer monitored online. In addition, the residual stresses introduced in laser cladding process also would depend on the thermo-cycle. This study could be further extended to establish correlation between residual stresses and the heating and cooling rates, and its effect on mechanical properties, such as fatigue life [45].

Conclusion

The thermo-cycle of molten pool during laser cladding of Inconel 718 and 30 % TiC MMC coating was monitored using an IR pyrometer and the effect of scan speed on its various features, *viz.* molten pool lifetime, solidification lifetime and cooling rate was studied. The condition of TiC particles in metal matrix, microstructure and phases of the clad layer, and the resulting mechanical properties were investigated for different scan speeds. Good correlation between different features of the thermo-cycle and various characteristics of the clad layer was observed. From these observations the following conclusions are drawn:

1. With the decrease of scan speed, the molten pool lifetime and solidification shelf time increases while cooling rate decreases.
2. Exposing TiC ceramic particles to high temperatures for relatively longer time results in decomposition of TiC particles.
3. The phase change in metal matrix composition due to the decomposition of TiC particles causes change in the solidification shelf which can be used as an effective indicator in online monitoring of ceramic particle condition in laser cladding process.
4. With the increase of molten pool lifetime, the reaction layer thickness between metal matrix and TiC particles increases to a certain limit after which TiC particles undergo complete decomposition forming dendritic structure and modifying the chemical and mechanical properties of the matrix.
5. Coatings with dendritic structure formed with decomposed TiC particles are brittle in nature exhibiting poor wear characteristics.

Acknowledgement

Authors gratefully acknowledge the financial support from the Department of Science and Technology, Ministry of Science and Technology, government of India, under the FIST Program-2007 (SR/FIST/ETII-031/2007).

References

- [1] J. Nurminen, J. Näkki, P. Vuoristo, Microstructure and properties of hard and wear resistant MMC coatings deposited by laser cladding, *Int. J. Refract. Met. Hard Mater.* 27 (2009) 472–478.
- [2] X.D. Hui, Y.S. Yang, Z.F. Wang, G.Q. Yuan, X.C. Chen, High temperature creep behavior of in-situ TiC particulate reinforced Fe–Cr–Ni matrix composite, *Mater. Sci. Eng. A* 282 (2000) 187–192.
- [3] H.Y. Wang, D.W. Zuo, G. Chen, G.F. Sun, X.F. Li, X. Cheng, Hot corrosion behaviour of low Al NiCoCrAlY cladded coatings reinforced by nano-particles on a Ni-base super alloy, *Corros. Sci.* 52 (2010) 3561–3567.
- [4] Z. Liu, J. Cabrero, S. Niang, Z.Y. Al-Taha, Improving corrosion and wear performance of HVOF-sprayed Inconel 625 and WC Inconel 625 coatings by high power diode laser treatments, *Surf. Coat. Technol.* 201 (2007) 7149–7158.
- [5] M. Sharifitabar, J. Vahdati Khaki, M. Haddad Sabzevar, Microstructure and wear resistance of in-situ TiC–Al₂O₃ particles reinforced Fe-based coatings produced by gas tungsten arc cladding, *Surf. Coat. Technol.* 285 (2016) 47–56.
- [6] J. Xu, B. Zou, S. Tao, M. Zhang, X. Cao, Fabrication and properties of Al₂O₃-TiB₂-TiC/Al metal matrix composite coatings by atmospheric plasma spraying of SHS powders, *J. Alloys Compd.* 672 (2016) 251-259.
- [7] G. Taillon, F. Pougoum, S. Lavigne, L. Ton-That, R. Schulz, E. Bousser, S. Savoie, L. Martinu, J. E. Klemberg-Sapieha, Cavitation erosion mechanisms in stainless steels and in composite metal–ceramic HVOF coatings, *Wear* 364-365 (2016) 201–210.
- [8] S. Y. Oh, J. A. Cornie, K. C. Russell, Wetting of ceramic particulates with liquid aluminum alloys: Part I. Experimental techniques, *Metall. Trans. A* 20 (1989) 527-532.
- [9] S. Y. Oh, J. A. Cornie, K. C. Russell, Wetting of ceramic particulates with liquid aluminum alloys: Part II. Study of wettability, *Metall. Trans. A* 20 (1989) 533-541.
- [10] J. Llorca, Fatigue of particle- and whisker-reinforced metal-matrix composites, *Prog. Mater. Sci.* 47 (2002) 283–353.

- [11] J. Nafar Dastgerdi, G. Marquis, S. Sankaranarayanan, M. Gupta, Fatigue crack growth behavior of amorphous particulate reinforced composites, *Compos. Struct.* 153 (2016) 782–790.
- [12] T. Rong, G. Dongdong, Formation of novel graded interface and its function on mechanical properties of WC_{1-x} reinforced Inconel 718 composites processed by selective laser melting, *J. Alloys Compd.* 680 (2016) 333–342.
- [13] C. Hong, D.D. Gu, D.H. Dai, A. Gasser, A. Weisheit, I. Kelbassa, M. Zhong, R. Poprawe, Laser metal deposition of TiC/Inconel 718 composites with tailored interfacial microstructures, *Opt. Laser Technol.* 54 (2013) 98–109.
- [14] Y. Zhang, Z. Li, P. Nie, Y. Wu, Carbide and nitride precipitation during laser cladding of Inconel 718 alloy coatings, *Opt. Laser Technol.* 52 (2013) 30–36.
- [15] F.J. Kahlen, A. Kar, Tensile Strengths for Laser-Fabricated Parts and Similarity Parameters for Rapid Manufacturing, *J. Manuf. Sci. Eng.* 123 (2001) 38–44.
- [16] S.K. Everton, M. Hirsch, P. Stravroulakis, R.K. Leach, A.T. Clare, Review of in-situ process monitoring and in-situ metrology for metal additive manufacturing, *Mater. Des.* 95 (2016) 431–445.
- [17] T. Purtonen, A. Kalliosaari, A. Salminen, Monitoring and adaptive control of laser processes, *Phys. Proc.* 56 (2014) 1218–1231.
- [18] M. Ignatiev, I. Smurov, G. Flamant, Real time optical pyrometry in laser machining, *Meas. Sci. and Technol.* 5 (1994) 563–573.
- [19] I. Smurov and M. Ignatiev, Real-time optical pyrometry in laser surface treatment, in: *Laser Processing: Surface Treatment and Film deposition*, NATO ASI Series, Series E: Applied Science, Ed. J. Mazumder (Kluwer, Dordrecht, 1995).
- [20] M.B. Ignatiev, I.Yu. Smurov, G. Flamant, V.N. Senchenko, Surface temperature measurements during pulsed laser action on metallic and ceramic materials, *Appl. Surf. Sci.* 96–98 (1996) 505–512.
- [21] M. Ignatiev, I.Yu. Smurov, G. Flamant, V. Senchenko, V. Dozhdikov, Two-dimensional resolution pyrometer for real-time monitoring of temperature image in laser materials processing, *Appl. Surf. Sci.* 109–110 (1997) 498–508.
- [22] M. Doubenskaia, Ph. Bertrand, I. Smurov, Optical monitoring of Nd:YAG laser cladding, *Thin Solid Films* 453–454 (2004) 477–485.
- [23] M. Doubenskaia, Ph. Bertrand, I. Smurov, Pyrometry in laser surface treatment, *Surf. Coat. Technol.* 201 (2006) 1955–1961.

- [24] G. Bi, A Gasser, K Wissenbach, A Drenker, P Poprawe, Identification and qualification of temperature signal for monitoring and control in laser cladding, *Opt. Laser. Eng.* 44 (2006) 1348–1359.
- [25] G. Bi, B. Schurmann, A. Gasser, K. Wissenbach, R. Poprawe, Development and qualification of a novel laser-cladding head with integrated sensors, *Int. J. Mach. Tool. Manu.* 47 (2007) 555–561.
- [26] G. Bi, A. Gasser, K. Wissenbach, A. Drenker, P. Poprawe, Characterization of the process control for the direct laser metallic powder deposition. *Surf. Coat. Tech.* 201 (2006) 2676–83.
- [27] H. J. Yu, T. He, C. Z. Chen, Research Progress in Laser Clad Nickel-Based Alloy Coatings, *Advanced Materials Research* 833 (2014) 252-256.
- [28] F. Weng, C. Chen, H. Yu, Research status of laser cladding on titanium and its alloys: a review, *Mater. Des.* 58 (2014) 412–425.
- [29] R.M. Mahamood, E.T. Akinlabi, M. Shukla, S. Pityana, Scanning velocity influence on microstructure, microhardness and wear resistance performance of laser deposited Ti6Al4V/TiC composite, *Mater. Des.* 50 (2013) 656–666.
- [30] D. Liu, P. Hu, G. Min, Interfacial reaction in cast WC particulate reinforced titanium metal matrix composites coating produced by laser processing, *Opt. Laser Technol.* 69 (2015) 180–186.
- [31] Q. Shi, D. Gu, M. Xia, S. Cao, T. Rong, Effects of laser processing parameters on thermal behavior and melting/solidification mechanism during selective laser melting of TiC/Inconel 718 composites, *Opt. Laser. Eng.* 84 (2016) 9–22.
- [32] N. Eliaz, G. Shemesh, R.M. Latanision, Hot corrosion in gas turbine components, *Eng. Fail. Anal.* 9 (2002) 31-43.
- [33] D.D. Gu, W. Meiners, K. Wissenbach, R. Poprawe, Laser additive manufacturing of metallic components: materials, processes and mechanisms, *Int. Mater. Rev.* 57 (2012) 133–164.
- [34] Q.B. Jia, D.D. Gu, Selective laser melting additive manufactured Inconel 718 superalloy parts: High-temperature oxidation property and its mechanisms, *Opt. Laser Technol.* 62 (2014) 161–171.
- [35] S. Yang, M.L. Zhong, W.J. Liu, TiC particulate composite coating produced in situ by laser cladding, *Mater. Sci. Eng. A* 343 (2003) 57–62.

- [36] A. Emamian, Stephen F. Corbin and A. Khajepour, In-Situ Deposition of Metal Matrix Composite in Fe-Ti-C System Using Laser Cladding Process, Dr. John Cuppoletti (Ed.), Metal, Ceramic and Polymeric Composites for Various Uses, (2011) 33-60.
- [37] C. K. Sahoo, M. Masanta, Effect of pulse laser parameters on TiC reinforced AISI 304 stainless steel composite coating by laser surface engineering process, Opt. Laser. Eng. 67 (2015) 36–48.
- [38] S. Anandan, S. Pityana, J. Dutta Majumdar, Structure–property–correlation in laser surface alloyed AISI 304 stainless steel with WC + Ni + NiCr, Mater. Sci. Eng. A 536 (2012) 159–169.
- [39] S. Zafar, A. Bansal, A. K. Sharma, N. Arora, C. S. Ramesh, Dry erosion wear performance of Inconel 718 microwave clad, Surf. Eng. 30 (2014) 852-859.
- [40] Y. K. Madhukar, S. Mullick, D. K. Shukla, S. Kumar, A. K. Nath. Effect of laser operating mode in paint removal with a fiber laser. Appl. Surf. Sci. 264 (2013) 892–901.
- [41] S.M. Thompson, L. Bian, N. Shamsaei, A. Yadollahi, An overview of Direct Laser Deposition for additive manufacturing; Part I: Transport phenomena, modeling and diagnostics, Addit. Manuf. 8 (2015) 36–62
- [42] S. Zhang, Y. L. Tian, F. J. Wang, Transient Temperature Field Analysis in Laser Cladding Processing, Adv. Mat. Res. 538-541 (2012) 1874-1877.
- [43] S. R. Shatynski, The Thermochemistry of transition metal carbides, Oxid. Metal. 13(2) (1979) 105-118.
- [44] A. Gaard, P. Krakhmalev, J. Bergstrom, Microstructural characterization and wear behavior of (Fe,Ni)–TiC MMC prepared by DMLS, J. Alloys Compd. 421 (2006) 166–171.
- [45] F. Brückner, D. Lepski, E. J. Beyer, Modeling the Influence of Process Parameters and Additional Heat Sources on Residual Stresses in Laser Cladding, J Therm Spray Tech 16 (2007) 355-373.

List of Figures

Fig. 1. Morphology of (a) Inconel 718 and (b) TiC powder

Fig. 2. Thermo-cycle recorded using IR pyrometer (without notch filter, 700 W, 9000 mm/min, 3 mm spot diameter)

Fig. 3. Typical profile of thermo-cycles (Without notch filter, 700 W, 3 mm spot diameter)

- Fig. 4.** Temperature signal recorded with notch filter (700 W, 2000 mm/min and 3 mm beam spot diameter)
- Fig. 5.** Molten pool thermal history in case of Al, Cu and SS 304
- Fig. 6.** Typical thermo-cycle recorded during laser cladding of Inconel 718 + TiC at 1200 W laser power and 200 mm/min scan speed
- Fig. 7.** Thermo-cycles during laser cladding of Inconel 718 and Inconel 718 + TiC at 1200 W laser power, (a) 1200 mm/min and (b) 400 mm/min
- Fig. 8.** Relation between slope of solidification shelf and microstructure
- Fig. 9.** Effect of scan speed on (a) Molten pool life time and solidification shelf life time and (b) cooling rate
- Fig. 10.** Variation in microstructure with molten pool life time (a) 0.281 s, (b) 0.3s, (c) 0.429 s, (d) 0.487 s, (e) 0.899 s and (f) 1.336 s
- Fig. 11.** Variation in reaction layer thickness with molten pool life time (a) 0.429 s, (b) 0.487 s, (c) 0.899 s and (d) 1.336 s
- Fig. 12.** Effect of scan speed on molten pool life time, cooling rate and reaction layer thickness
- Fig. 13.** Elemental mapping of TiC particle (1200 W, 1000 mm/min)
- Fig. 14.** Elemental mapping of Nb and Ti in fully grown dendritic structure (1200 W, 400 mm/min)
- Fig. 15.** XRD peaks of (a) TiC particles and clad tracks deposited at (a) 1200 mm/min, (b) 800 mm/min and (c) 400 mm/min
- Fig. 16.** Fracture surface of samples cladded at 1200 W laser power and (a) 1200 mm/min and (b) 400 mm/min scan speed
- Fig. 17.** Variation of wear rate with scan speed and molten pool life time
- Fig. 18.** SEM images showing typical wear surface morphology of samples cladded at 1200 W laser power and (a), (b) 1200 mm/min and (c), (d) 400 mm/min scan speed and (e), (f) corresponding debris

List of tables




Table 1

Chemical composition (Wt%) of cladding and substrate materials

Table 2

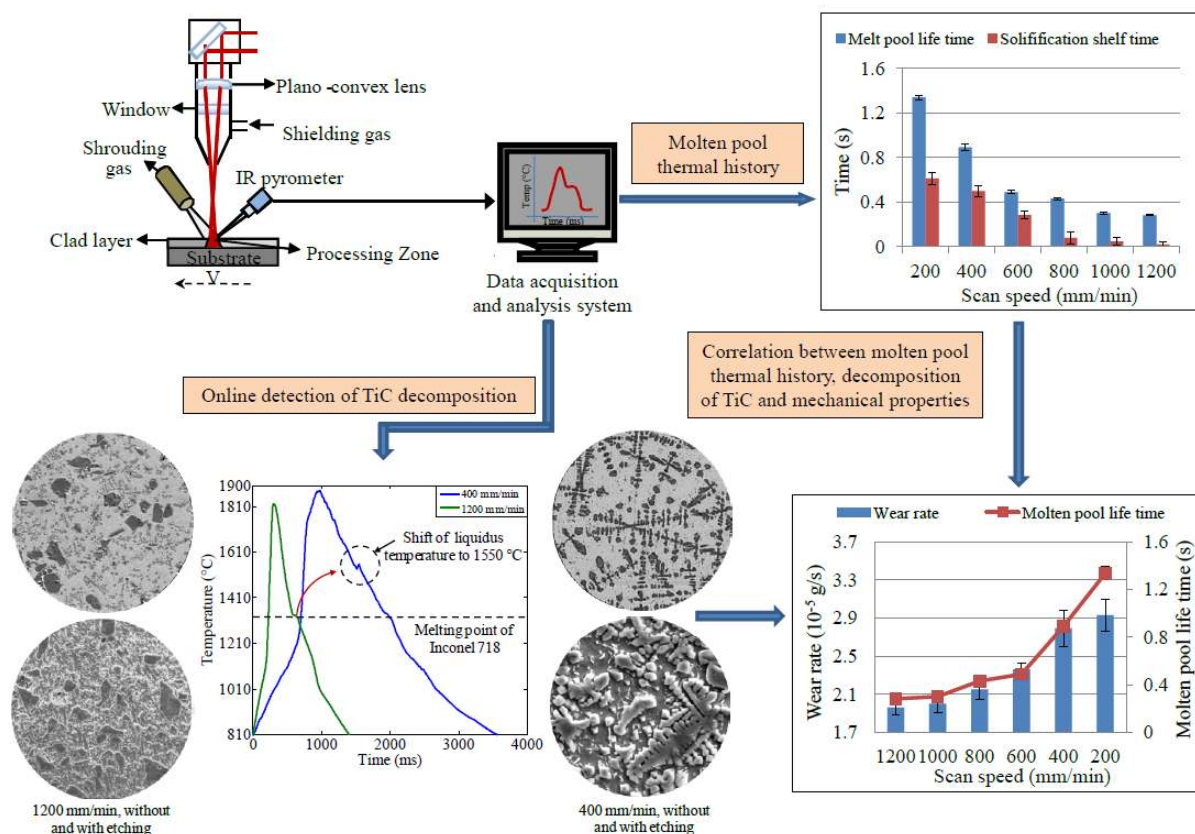
Laser cladding process parameters

Vitae

	<p>Muvvala Gopinath is currently a Ph.D. student in the Department of Mechanical Engineering of Indian Institute of Technology, Kharagpur. He is working in the area of ‘Laser additive manufacturing’ and also on ‘Laser surface modification’. He obtained his M.Tech. degree in Manufacturing Science and Engineering in 2013 from the same institute, and B.Tech degree in Mechanical Production and Industrial Engineering from GITAM University, Visakhapatnam, India in 2011. He has co-authored several conference papers in the area of laser cladding.</p>
	<p>Debapriya Patra Karmakar is currently a Ph.D. student in the Department of Mechanical Engineering of Indian Institute of Technology, Kharagpur. He is working in the area of ‘Laser cladding of hardfacing alloy on hot-work tool steel’ and also on ‘Laser surface modification’. He obtained his M. Tech degree in Manufacturing Science and Engineering in 2013 from the same institute, and B.E. degree from Bengal Engineering and Science University, Shibpur (currently known as IEST, Shibpur), India in 2011.</p>
	<p>Dr. Nath started his scientific career in BARC, Mumbai, India after graduating from BARC Training School in 1972. He worked mainly on the development of high power lasers and their scientific and industrial applications. He obtained Doctoral degree in 1982. He was a PDF in University of Alberta, Canada during 1982-84. During 1986-‘07 he headed Industrial CO₂ laser Program and also Solid State and Semiconductor Lasers Program (2005-‘07) in RRCAT, Indore. Since 2008 he is a Professor in Mechanical Engineering Department, IIT Kharagpur. He has co-authored more than 135 journal papers. His present research interests include laser additive manufacturing and process monitoring, laser surface engineering, and underwater laser material processing.</p>

ACCEPTED MANUSCRIPT

Graphical abstract



Highlights

- Thermal history of molten pool in laser cladding of Inconel 718 + TiC metal matrix composite coating was monitored online using an IR pyrometer
- TiC decomposition was detected from IR pyrometer signal and a parametric study was carried out
- Correlation between molten pool life time, TiC decomposition and its effect on microstructure and mechanical properties was studied.

ACCEPTED MANUSCRIPT